

# Two (2 + 1)-dimensional integrable nonlocal nonlinear Schrödinger equations: Breather, rational and semi-rational solutions

Yulei Cao<sup>a</sup>, Boris A. Malomed<sup>b,c</sup>, Jingsong He<sup>a,\*</sup>

<sup>a</sup>Department of Mathematics, Ningbo University, Ningbo, Zhejiang, 315211, P. R. China

<sup>b</sup>Department of Physical Electronics, Faculty of Engineering, Tel Aviv University, Tel Aviv 69978, Israel

<sup>c</sup>Laboratory of Nonlinear-Optical Informatics, ITMO University, St. Petersburg 197101, Russia

---

## Abstract

Recently, an integrable system of coupled (2 + 1)-dimensional nonlinear Schrödinger (NLS) equations was introduced by Fokas (eq. (18) in *Nonlinearity* **29**, 319324 (2016)). Following this pattern, two integrable equations [eqs.(2) and (3)] with specific parity-time symmetry are introduced here, under different reduction conditions. For eq. (2), two kinds of periodic solutions are obtained analytically by means of the Hirota's bilinear method. In the long-wave limit, the two periodic solutions go over into rogue waves (RWs) and semi-rational solutions, respectively. The RWs have a line shape, while the semi-rational states represent RWs built on top of the background of periodic line waves. Similarly, semi-rational solutions consisting of a line RW and line breather are derived. For eq. (3), three kinds of analytical solutions, *viz.*, breathers, lumps and semi-rational solutions, representing lumps, periodic line waves and breathers are obtained, using the Hirota method. Their dynamics are analyzed and demonstrated by means of three-dimensional plots. It is also worthy to note that eq. (2) can reduce to a (1 + 1)-dimensional "reverse-space" nonlocal NLS equation by means of a certain transformation. Lastly, main differences between solutions of eqs.(2) and (3) are summarized.

**Keywords:**  $\mathcal{PT}$ -symmetry · Bilinear method · Breather solution · Rational solution · Semi-rational solution

**2010 MSC:** 35C08, 35Q51, 37K10, 37K35

---

## 1. Introduction

Rogue waves (RWs) have become famous due to their realization as spontaneously emerging freak surface waves in the ocean (where they are held responsible for some maritime disasters). In this context, they are often characterized as localized patterns which "appear from nowhere and then disappear without a trace" [1]. RWs have been identified in a number of other contexts, including Bose-Einstein condensates [2, 3], optical systems [4, 5], oceanography [6], plasmas [7, 8], etc. The Peregrine soliton is the fundamental (first-order) RW solution produced by the one-dimensional (1D) nonlinear Schrödinger (NLS) equation [9]. Lately, higher-order RW solutions of the NLS equation have been produced by different methods [10, 11, 12, 13, 14, 15, 16]. Moreover, a series of other soliton equations have also been shown to possess RW solutions [17, 18, 19, 20, 21, 22, 23, 24]. Detailed reviews of theoretical and experimental aspects of RWs are available in Refs. [25, 26, 27]. Due to the fact that the ocean surface is two-dimensional (2D), studies of RWs have been naturally extended from 1D to 2D models. In particular, RW solutions of several important integrable 2D equations have been derived explicitly, such as the Davey-Stewartson (DS) [28, 29] and Kadomtsev-Petviashvili-I (KP I) [26, 30] equations, and others [31, 32, 33, 34]. Similar solutions were found even in the 3D KP equation [35].

It is relevant to mention that RWs are essentially unstable solutions, as they are supported by the modulationally unstable background. An interesting possibility is to effectively stabilize RW-like modes by means of the nonlinearity- and dispersion- "management" techniques [36], even if the integrability of the underlying NLS equation is lost in such a setting.

---

\* e-mail: hejingsong@nbu.edu.cn; jshe@ustc.edu.cn

Recently, Fokas [37] has found an integrable system of coupled 2D NLS equations,

$$\begin{aligned} iU_t + U_{xy} - \frac{1}{2}(\partial_z^{-1} + \partial_{\bar{z}}^{-1})U[UV]_y &= 0, \\ iV_t - V_{xy} + \frac{1}{2}(\partial_z^{-1} + \partial_{\bar{z}}^{-1})V[UV]_y &= 0, \end{aligned} \quad (1)$$

obtained as a special reduction to a more general  $(4 + 2)$ -dimensional system [38]; here,  $z \equiv x + iy$ , and  $\partial_{z,\bar{z}}^{-1}$  are operators inverse to  $\partial_z \equiv (1/2)(\partial_x - i\partial_y)$  and  $\partial_{\bar{z}} \equiv (1/2)(\partial_x + i\partial_y)$ ; in particular,  $\partial_z^{-1} = \iint (z - z')^{-1} f(x', y') dx' dy'$ . Here,  $U$  and  $V$  are complex functions of  $x, y$  and  $t$ .

If  $y = x$ , then  $\partial_z^{-1} + \partial_{\bar{z}}^{-1} = \partial_x^{-1}$  and eq. (1) reduces to the classical system of AKNS equations [39]. Eq. (1) becomes the following integrable ‘‘reverse-space’’ 2D nonlocal NLS equation [37] when  $V(x, y, t) = \lambda U^*(-x, -y, t)$ , and  $\lambda = \pm 1$ :

$$(i\partial_t + \partial_{xy}^2)U(x, y, t) - \frac{\lambda}{2}U(x, y, t)(\partial_z^{-1} + \partial_{\bar{z}}^{-1})\partial_y[U(x, y, t)U^*(-x, -y, t)] = 0, \lambda = \pm 1, \quad (2)$$

If  $V(x, y, t) = \lambda U^*(-x, y, -t)$ ,  $\lambda = \pm 1$ , a reverse space-time nonlocal NLS equation is introduced:

$$(i\partial_t + \partial_{xy}^2)U(x, y, t) - \frac{\lambda}{2}U(x, y, t)(\partial_z^{-1} + \partial_{\bar{z}}^{-1})\partial_y[U(x, y, t)U^*(-x, y, -t)] = 0, \lambda = \pm 1, \quad (3)$$

Eqs. (2) and (3) satisfy the condition of the 2D parity-time ( $\mathcal{PT}$ ) symmetry. The concept of the  $\mathcal{PT}$  symmetry in the quantum theory has been introduced in pioneering works which aimed to construct non-Hermitian Hamiltonians with real spectra [40, 41]. Various states generated by  $\mathcal{PT}$ -symmetric systems are supported by the balance of loss and gain inherent to this symmetry [42, 43], see comprehensive review [44]. Many results for nonlinear  $\mathcal{PT}$ -symmetric models, where the gain-loss balance is combined with the usual equilibrium between diffraction and nonlinear self-interaction, were summarized in reviews [44] and [45]. The  $\mathcal{PT}$ -symmetry has also been studied extensively in multi-dimensional systems [45, 46, 47, 48, 49, 50]. An issue of obvious interest is to produce multi-dimensional integrable models featuring the  $\mathcal{PT}$  symmetry, which is a motivation for the consideration of eqs. (2) and (3), and to explore dynamics of RWs in  $\mathcal{PT}$ -symmetry.

The rest of the paper is organized as follows. In sec. 2, periodic line-wave, RW, and semi-rational solutions, composed of first-order RWs, line breathers and periodic line waves of eq. (2) are produced by means of the Hirota method. In the same section, typical dynamics of these solutions are analyzed and demonstrated. In sec. 3, three kinds of analytical solutions of eq. (3), namely, breathers, lumps and semi-rational solutions, consisting of lump modes, periodic line waves, and breathers are derived and illustrated. The main results of the paper are summarized in sec. 4.

## 2. Solutions of the reverse-space nonlocal 2D NLS equation(2)

In this section, we focus on eq. (2). Setting

$$V_x = [U(x, y, t)U^*(-x, -y, t)]_y, \quad (4)$$

Eq. (2) becomes the following system of coupled partial differential equations:

$$\begin{aligned} iU_t + U_{xy} + UV &= 0, \\ V_x &= [U(x, y, t)U^*(-x, -y, t)]_y, \end{aligned} \quad (5)$$

Here  $U$  and  $V$  are two complex functions of  $x, y$  and  $t$ , and  $V$  satisfies the two-dimensional PT symmetry condition  $V(x, y, t) = V^*(-x, -y, t)$ . This observation inspires us to study (2) or equivalent (5). employing the bilinear method. To this end, the equation can be translated into the following bilinear form:

$$\begin{aligned} (D_x D_y + iD_t)g \cdot f &= 0, \\ (D_x^2 + 1)f \cdot f &= gg^*(-x, -y, t), \end{aligned} \quad (6)$$

through the transformation of the dependent variables:

$$U = g/f, \quad V = 2(\ln f)_{xy}, \quad (7)$$

where  $f$  and  $g$  are functions of  $x, y$  and  $t$ , subject to the condition:

$$f(x, y, t) = f^*(-x, -y, t). \quad (8)$$

$D$  is the Hirota's bilinear differential operator [51] defined by

$$P(D_x, D_y, D_t)F(x, y, t \cdots) \cdot G(x, y, t, \cdots) \quad (9)$$

$$= P(\partial_x - \partial_{x'}, \partial_y - \partial_{y'}, \partial_t - \partial_{t'}, \cdots)F(x, y, t, \cdots)G(x', y', t', \cdots)|_{x'=x, y'=y, t'=t}, \quad (10)$$

where  $P$  is a polynomial of  $D_x, D_y, D_t, \cdots$ .

The  $N$ -soliton solutions  $U$  and  $V$  given in (7) of the eq. (2) can be obtained by the bilinear transform method [51], in which  $f$  and  $g$  are written in the following forms:

$$f = \sum_{\mu=0,1} \exp\left(\sum_{j<k}^{(N)} \mu_j \mu_k A_{jk} + \sum_{j=1}^N \mu_j \eta_j\right), \quad g = \sum_{\mu=0,1} \exp\left(\sum_{j<k}^{(N)} \mu_j \mu_k A_{jk} + \sum_{j=1}^N \mu_j (\eta_j + i\Phi_j)\right). \quad (11)$$

Here

$$\begin{aligned} \Omega_j &= -Q_j \sqrt{-P_j^2 + 2}, \eta_j = iP_j x + iQ_j y + \Omega_j t + \eta_j^0, \cos \Phi_j = -P_j^2 + 1, \\ \sin \Phi_j &= \sqrt{(-P_j^2 + 2)P_j}, \exp(A_{jk}) = -\frac{\cos(\Phi_j - \Phi_k) + (P_j - P_k)^2 - 1}{\cos(\Phi_j + \Phi_k) + (P_j + P_k)^2 - 1}, \end{aligned} \quad (12)$$

where  $P_j, Q_j$ , are arbitrary real parameters, and  $\eta_j^0$  are complex constants. The notation  $\sum_{\mu=0,1}$  implies summation over all possible combinations of  $\mu_1 = 0, 1, \mu_2 = 0, 1, \cdots, \mu_n = 0, 1$ . The  $\sum_{j<k}^N$  summation is performed over all possible combinations of the  $N$  elements, subject to condition  $j < k$ .

### 2.1. periodic line wave solutions

Following previous works [52, 53, 54, 55],  $n$ -th-order line breather solutions of the eq. (2) can be generated by taking parameters in eq.(11) as

$$N = 2n, P_j = -P_{n+j}, Q_j = -Q_{n+j}, \eta_j^0 = \eta_{n+j}^0. \quad (13)$$

For instance, a particular case of eq. (13), with

$$N = 2, P_1 = -P_2, Q_1 = -Q_2, \eta_1^0 = \eta_2^0 = 0, \quad (14)$$

produces the first-order breather solution which is shown in Fig. 1. It is seen that the corresponding solution describes a periodic array of line waves in the  $(x, y)$  plane, first growing and then decaying in time. Five panels in Fig. 1 show that the first-order line breather appears at  $t < 0$  from a flat background, gradually attains a maximum amplitude at  $t = 0$ , and finally returns back to the asymptotic background without a trace, which is typical to RWs.

Additionally, for the case of  $N = 2n + 1$ , another type of periodic solutions composed of line breathers and periodic line waves can be generated via eq. (7), taking parameters

$$N = 2n + 1, P_j = -P_{n+j}, Q_j = -Q_{n+j}, \eta_j^0 = \eta_{n+j}^0, P_{2n+1} Q_{2n+1} \neq 0 \quad (15)$$

in eq. (11). For example, setting

$$N = 3, P_1 = -P_2, Q_1 = -Q_2, P_3 = -Q_3, \eta_1^0 = \eta_2^0, P_3 Q_3 \neq 0, \quad (16)$$

in eq. (15), we obtain a mixed solution composed of the first-order line breather and first-order periodic line wave. The dynamics of the emergence and disappearance of this third-order solution is shown in Fig. 2. It is seen that the

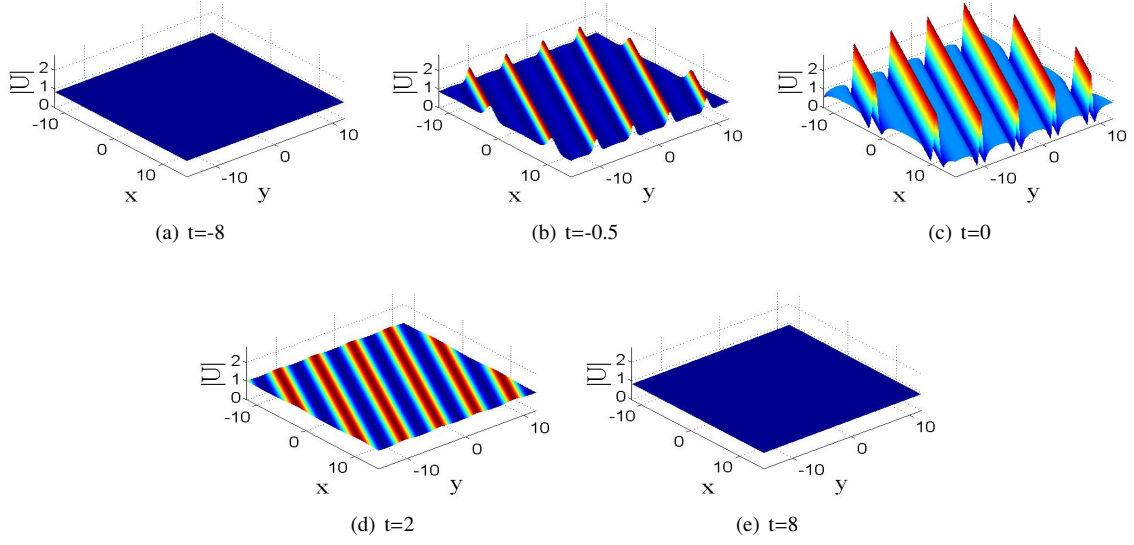


Figure 1: The evolution of the first-order line breather of eq. (2) in the  $(x, y)$ -plane, corresponding to parameters  $P_1 = \frac{1}{2}$  and  $Q_1 = 1$  in eq. (14).

first-order periodic line wave arises from the constant background at  $t < -16$ , which possesses one maximum and one minimum amplitude, featuring a clear parallel-line profile in the horizontal direction (see Fig.2b). Subsequently, the first-order line breather appears in the vertical direction, overlaid on the periodic line wave around  $t = -1$ . Due to the amplitude of the periodic line waves are too small, so the interaction phenomenon of periodic line waves and line breather are covered up. Along the evolution in time the characteristic of the line breather becomes clearer, which has one maximum and two minimum amplitudes (See Fig.2d, it is similar to Fig.1c), and the phenomenon of interaction is also gradually obvious at  $t = 0$ , then an array of sharp peaks is observed at  $t = 2$ , produced by the interplay of the two wave patterns. Next, the first-order line breather quickly merges back into background, but the first-order periodic line wave is observed around  $t = 4$ . Finally, this periodic line-wave pattern disappears at  $t > 8$ . Note that this 2D dynamical solution is different from the one obtained by means of the same method in the nonlocal DS I and II equations [52, 53]. Further, it is relevant to mention that Fig. 2(d) is similar to the doubly periodic line wave in the  $(x, t)$  (rather than  $(x, y)$ ) plane, obtained in [56] (see Fig.1(c) in that work).

## 2.2. Rational and semi-rational solutions.

To generate RW solutions of eq. (2), the long-wave limit of the breather solutions given by eq. (11) may be used. Indeed, taking parameters in eq. (11) as

$$N = 2, Q_1 = \lambda_1 P_1, Q_2 = \lambda_2 P_2, \lambda_1 = \lambda_2 = \lambda \neq 0, \quad (17)$$

and taking the limit of  $P_j \rightarrow 0$  ( $j = 1, 2$ ), the first-order RW solution is obtained as

$$\begin{aligned} U &= \frac{(\theta_1 + b_1)(\theta_2 + b_2) + \alpha_{12}}{\theta_1 \theta_2 + \alpha_{12}} = \frac{2(\lambda y + x)^2 + 4(\lambda t - i)^2 + 1}{2(\lambda y + x)^2 + 4(\lambda t)^2 + 1}, \\ V &= 2(\ln(\theta_1 \theta_2 + \alpha_{12}))_{xy} = \frac{2\lambda_1[-2(\lambda y + x)^2 + 4(\lambda t)^2 + 1]}{[(\lambda y + x)^2 + 2(\lambda t)^2 + \frac{1}{2}]^2}, \end{aligned} \quad (18)$$

where

$$\theta_j = i\lambda_j y - \sqrt{2}\lambda_j t + ix, b_1 = -b_2 = i\sqrt{2}, \alpha_{12} = -\frac{1}{2}, \quad (19)$$

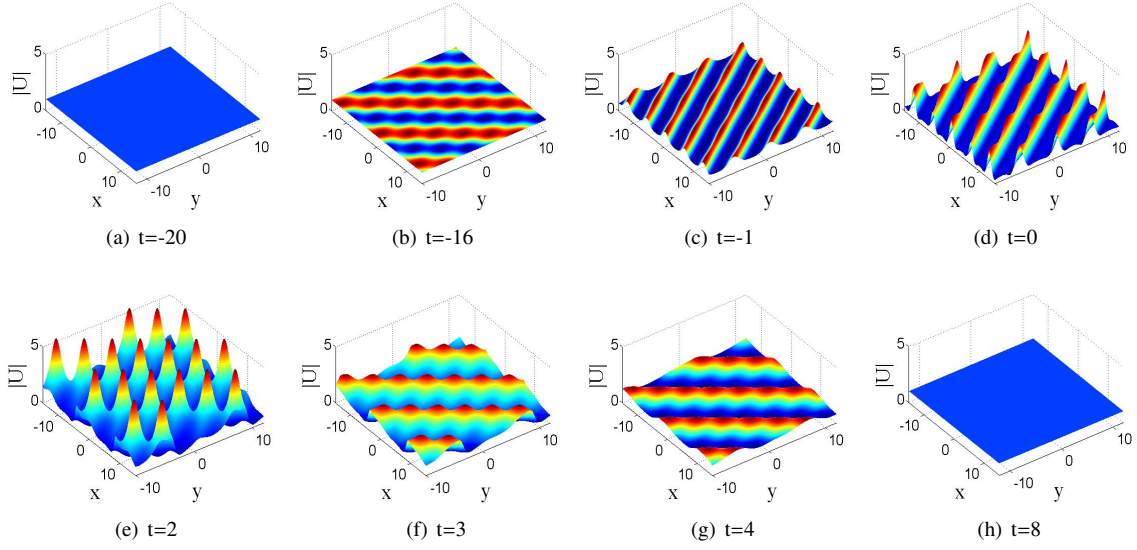


Figure 2: The evolution of the third-order periodic solution  $|U|$  of eq. (2) in the  $(x, y)$ -plane, with parameters  $P_1 = 1, Q_1 = 1, P_3 = \frac{1}{2}$ , and  $\eta_1^0 = 0, \eta_3^0 = -\frac{\pi}{2}$  in eq. (16).

with the corresponding profile of  $|U(x, y)|$  shown in Fig.3. It is seen that this W-shaped solution describes an emerging and decaying line wave oriented in the  $(\lambda, -1)$  direction of the  $(x, y)$ -plane. At any given time, this solution keeps a constant value along the line direction defined by  $\lambda y + x = 0$ , and  $|U(x, y)|$  uniformly approaches the flat background at  $t \rightarrow \pm\infty$ . At finite times,  $|U(x, y)|$  attains a maximum at the center ( $\lambda y + x = 0$ ) of the line wave. In particular, the maximum value is 3 (i.e., three times the background amplitude) at  $t = 0$ . We stress that the rational solution given by Eq. (18) can not be directly reduced to rational solutions of the  $\mathcal{PT}$  symmetric DS I equation found in Ref. [52, 53].

Furthermore, semi-rational solutions of eq. (2) can be obtained by taking the long-wave limit of periodic solutions, which describe the interplay of RWs with periodic waves. Indeed, setting parameters in eq. (11) to be

$$0 < 2j < N, 1 \leq k \leq 2j, Q_k = \lambda_k P_k, \eta_k^0 = i\pi, \quad (20)$$

and taking the limit of  $P_k \rightarrow 0$ , functions  $f$  and  $g$  defined by eq. (11) become a combination of polynomial and exponential functions, which generate a semi-rational solution for  $U(x, y, t)$  and  $V(x, y, t)$  of eq. (2) via eq. (7).

To clearly illustrate this method for constructing the semi-rational solutions, we take here  $N = 3$  and  $\Omega_3 = 0$ . Setting

$$Q_k = \lambda_k P_k, \quad \eta_k^0 = i\pi (k = 1, 2), \quad (21)$$

and taking the limit of  $P_k \rightarrow 0$  in eq. (11), we obtain

$$\begin{aligned} f &= (\theta_1 \theta_2 + a_{12}) + (\theta_1 \theta_2 + a_{12} + a_{13} \theta_2 + a_{23} \theta_1 + a_{12} a_{23}) e^{\eta_3}, \\ g &= [(\theta_1 + b_1)(\theta_2 + b_2) + a_{12}] + [(\theta_1 + b_1)(\theta_2 + b_2) + a_{12} + a_{13}(\theta_2 + b_2) \\ &\quad + a_{23}(\theta_1 + b_1) + a_{12} a_{23}] e^{\eta_3 + i\phi_3}, \end{aligned} \quad (22)$$

where  $a_{j3} = 1 - 2p_j P_3 \left[ \sqrt{2(-P_3^2 + 2)} + 2 \right]^{-1}$ ,  $\delta_j, \delta_j = \pm 1$  ( $j = 1, 2$ ), and  $a_{12}, b_j, \Phi_j, \eta_3$  are given by eqs. (12) and (19). The corresponding semi-rational solution is shown in Fig. 4. It is seen that it describes a line RW on top of the background of periodic line waves. When  $t \rightarrow \pm\infty$ , the line RW approaches the background, see the panels corresponding to  $t = \pm 5$ . At the intermediate time moment,  $t = -0.35$ , the line RW arises from the periodic background, then the interplay around  $t = 0$  between the line RW and the periodic line-waves background creates sharp peaks along the line RW, which can reach the maximum value of 8 (i.e., 8 times the background amplitude). In

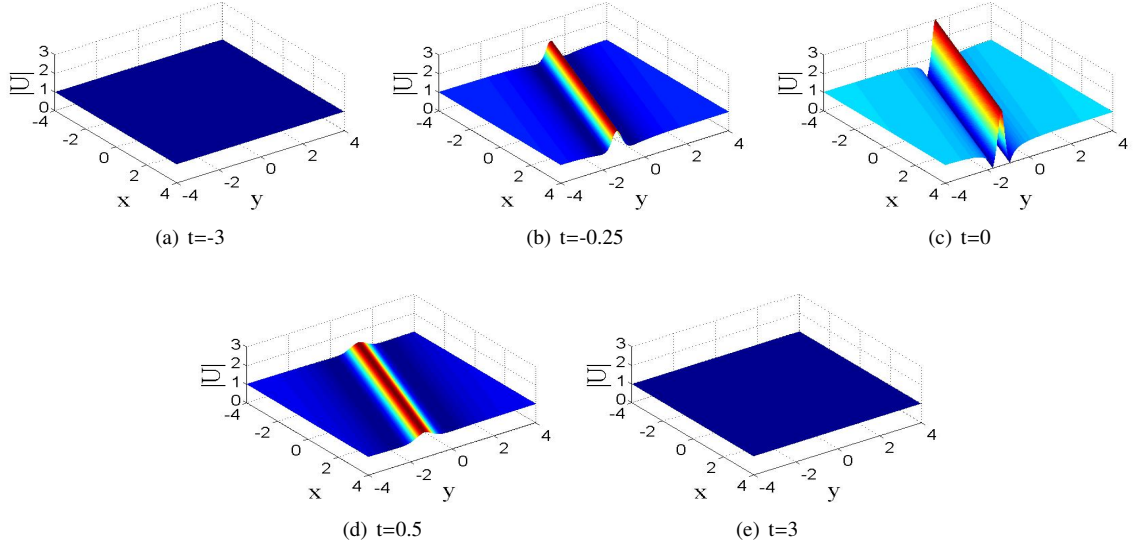


Figure 3: The time evolution of the first-order (W-shaped) line rogue wave in the  $(x, y)$  plane, given by solution (18), (19) of eq. (2), with parameter  $\lambda = 3$  in eq. (17).

the course of the subsequent evolution, all peaks on the line RW gradually merge into periodic line waves. Finally, the wave field returns to the background formed by the periodic line waves at  $t \rightarrow \infty$ . This solution is, in particular, notably different from the corresponding solutions with the flat background of the nonlocal DS I equation presented in Ref. [52], see Fig. 12 in that work.

Furthermore, higher-order semi-rational solutions consisting of RW and line breather solutions can also be generated in a similar way for larger values of  $N$ . We have to take the parameters

$$N = 4, Q_1 = \lambda_1 P_1, Q_2 = \lambda_2 P_2, \eta_1^0 = \eta_2^0 = i\pi, \eta_3^0 = \eta_4^0, \quad (23)$$

and take a limit as  $P_1, P_2 \rightarrow 0$ . Then the functions  $f$  and  $g$  can be rewritten as

$$\begin{aligned} f &= e^{A_{34}}(a_{13}a_{23} + a_{13}a_{24} + a_{13}\theta_2 + a_{14}a_{23} + a_{14}a_{24} + a_{14}\theta_2 + a_{23}\theta_1 + a_{24}\theta_1 + \theta_1\theta_2 \\ &\quad + a_{12})e^{\eta_3 + \eta_4} + (a_{13}a_{23} + a_{13}\theta_2 + a_{23}\theta_1 + \theta_1\theta_2 + a_{12})e^{\eta_3} + (a_{14}a_{24} + a_{14}\theta_2 + a_{24}\theta_1 \\ &\quad + \theta_1\theta_2 + a_{12})e^{\eta_4} + \theta_1\theta_2 + a_{12}, \\ g &= e^{A_{34}}[a_{13}a_{23} + a_{13}a_{24} + a_{13}(\theta_2 + b_2) + a_{14}a_{23} + a_{14}a_{24} + a_{14}(\theta_2 + b_2) + a_{23}(\theta_1 + b_1) \\ &\quad + a_{24}(\theta_1 + b_1) + (\theta_1 + b_1)(\theta_2 + b_2) + a_{12}]e^{\eta_3 + i\phi_3 + \eta_4 + i\phi_4} + [a_{13}a_{23} + a_{13}(\theta_2 + b_2) \\ &\quad + a_{23}(\theta_1 + b_1) + (\theta_1 + b_1)(\theta_2 + b_2) + a_{12}]e^{\eta_3 + i\phi_3} + [a_{14}a_{24} + a_{14}(\theta_2 + b_2) + a_{24}(\theta_1 \\ &\quad + b_1) + (\theta_1 + b_1)(\theta_2 + b_2) + a_{12}]e^{\eta_4 + i\phi_4} + (\theta_1 + b_1)(\theta_2 + b_2) + a_{12}, \end{aligned} \quad (24)$$

Here  $a_{jk} = \delta_j \frac{\sqrt{2}P_j P_k}{\sqrt{-P_k^2 + 2 + \sqrt{2}\delta_k}}$ ,  $\delta_j \delta_k = -1$ ,  $\theta_j, \alpha_{12}$  and  $\phi_l, \eta_l, A_{34}$  are given by eqs.(12) and (19), respectively. Further,

we take

$$\lambda_1 = \lambda_2 = 1, P_3 = -P_4 = 2, Q_3 = -Q_4 = \frac{1}{3}, \eta_3^0 = \eta_4^0 = -\frac{3\pi}{2}. \quad (25)$$

thus, the corresponding semi-rational solutions  $|U|$ , consisting of a line rogue wave and line breather, are obtained analytically. As can be seen in Fig.5, the first-order line rogue wave arise from the background of first-order line breather and disappear into the same background, and this process lasts only for a short time. Specifically, compared to Fig.4 line rogue waves on the background of the line breather do not generate high peaks(see Fig. 5c).

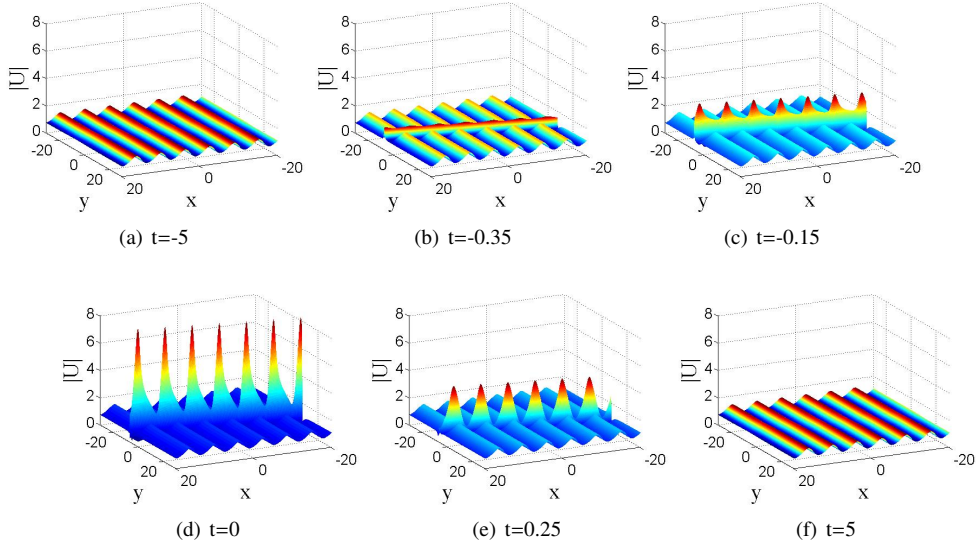


Figure 4: The evolution of the line RW on top of the background formed by periodic line waves with parameters  $\lambda_1 = \lambda_2 = 3$ ,  $Q_3 = 0$ ,  $P_3 = 1$ , and  $\eta_3^0 = -\pi/2$  in eq. (21).

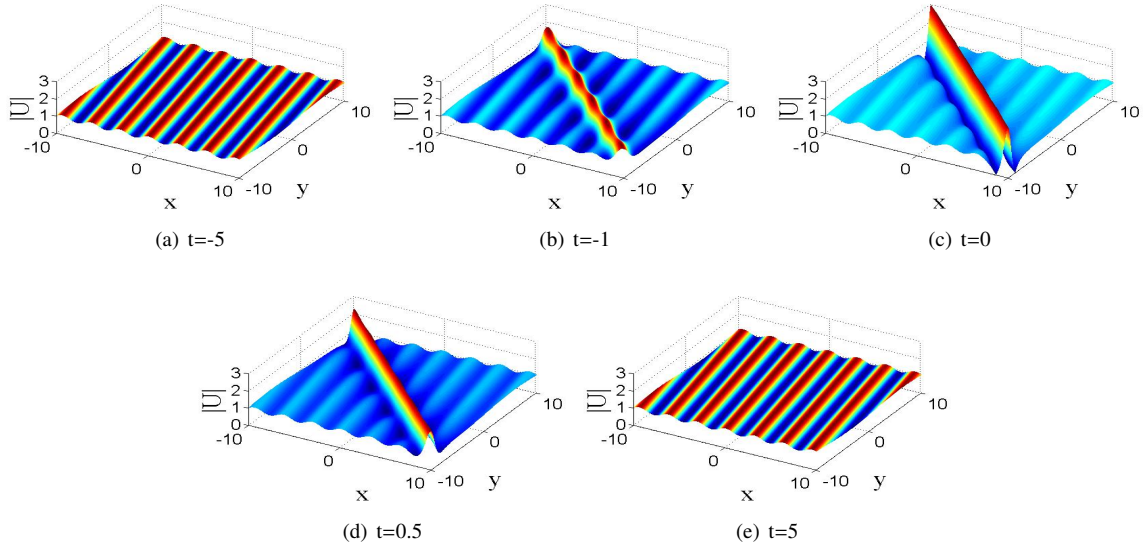


Figure 5: The evolution of the solution to eq. (2) in the form of the line rogue wave, built on top of the line-breather background, in the  $(x, y)$ -plane

### 2.3. A Reduction of the reverse-space nonlocal 2D NLS equation (2)

It is universally acknowledged that 1D nonlocal NLS equation plays an important part in nonlinear systems. It was first introduced by Ablowitz[57], and then has been paid intensive researches on its integrable properties and solutions[58, 59, 60, 61, 62, 63]. Lately, 1D nonlocal NLS equation was obtained in a physical application of magnetics[64]. Subsequently, several extension visions to 1D nonlocal NLS equation were introduced[37, 65]. Furthermore, 2D NLS equation is the high-dimensional version of 1D NLS equation. The natural question is whether 2D NLS equation can reduce to 1D NLS equation?

Setting  $X = \alpha x + \beta y$ ,  $T = t$ , eq. (5) can be reduced to the following standard 1D reverse-space nonlocal NLS

equation:

$$iU(X, T)_T + \alpha\beta U(X, T)_{XX} + \frac{\beta}{\alpha} U(X, T)U(X, T)U(-X, T) = 0, \quad (26)$$

where  $\alpha$  and  $\beta$  are arbitrary real constants. Eq. (26) is called the ‘‘self-focusing’’ for  $\alpha\beta > 0$  and ‘‘defocussing’’ for  $\alpha\beta < 0$ , respectively. Given the solution of eq. (26), we can get a solution of eq. (5). In other words, given the solution of (5), we can get the solution of eq. (26) analytically.

### 3. Reverse space-time nonlocal 2D NLS equation (3)

In this section, solutions of the reverse space-time nonlocal eq. (3) are considered by means of the bilinear method. Similarly, eq.(3) can be rewritten as the following bilinear form:

$$\begin{aligned} (D_x D_y + iD_t)\tilde{g} \cdot \tilde{f} &= 0, \\ (D_x^2 + 1)\tilde{f} \cdot \tilde{f} &= \tilde{g}\tilde{g}^*(-x, y, -t), \end{aligned} \quad (27)$$

through the dependent variable transformation:

$$U = \tilde{g}/\tilde{f}, \quad V = 2(\log \tilde{f})_{xy}, \quad (28)$$

where  $\tilde{f}$  and  $\tilde{g}$  are functions with respect to three variables  $x, y$  and  $t$ , and satisfy the condition:

$$V_x = [U(x, y, t)U^*(-x, y, -t)]_y, \quad \tilde{f}(x, y, t) = \tilde{f}^*(-x, y, -t). \quad (29)$$

The operator  $D$  is the Hirota’s bilinear differential operator[51] defined by

$$\begin{aligned} &P(D_x, D_y, D_t, \dots)F(x, y, t, \dots) \cdot G(x, y, t, \dots) \\ &= P(\partial_x - \partial_{x'}, \partial_y - \partial_{y'}, \partial_t - \partial_{t'}, \dots)F(x, y, t, \dots)G(x', y', t', \dots)|_{x'=x, y'=y, t'=t}, \end{aligned}$$

where  $P$  is a polynomial of  $D_x, D_y, D_t, \dots$ .

The  $N$ -soliton solutions  $U$  and  $V$  of eq. (3) can be obtained by the bilinear transform method [51] using (27) and (28), in which  $\tilde{f}$  and  $\tilde{g}$  are written in the following forms:

$$\tilde{f} = \sum_{\mu=0,1} \exp\left(\sum_{k<j}^N \mu_k \mu_j \tilde{A}_{kj} + \sum_{k=1}^N \mu_k \tilde{\eta}_k\right); \quad \tilde{g} = \sum_{\mu=0,1} \exp\left(\sum_{k<j}^N \mu_k \mu_j \tilde{A}_{kj} + \sum_{k=1}^N \mu_k (\tilde{\eta}_k + i\tilde{\Phi}_k)\right), \quad (30)$$

Here

$$\begin{aligned} \tilde{\Omega}_j &= Q_j \sqrt{-P_j^2 + 2}; \tilde{\eta}_k = iP_j x + Q_j y + i\tilde{\Omega}_j t + \eta_j^0; \cos \tilde{\Phi}_j = -P_j^2 + 1, \\ \sin \tilde{\Phi}_j &= \sqrt{(-P_j^2 + 2)P_j}; \exp(\tilde{A}_{jk}) = -\frac{\cos(\tilde{\Phi}_j - \tilde{\Phi}_k) + (P_j - P_k)^2 - 1}{\cos(\tilde{\Phi}_j + \tilde{\Phi}_k) + (P_j + P_k)^2 - 1}, \end{aligned} \quad (31)$$

#### 3.1. Periodic solutions

Similarly, the  $n$ th-order breather solutions of eq. (3) can be generated by taking the set of parameters in eq. (30).

$$N = 2n, P_j = -P_k, Q_j = Q_k, \eta_j^0 = \eta_k^0, \quad (32)$$

For example, we take

$$N = 2, P_1 = -P_2, Q_1 = Q_2, \eta_1^0 = \eta_2^0 = 0, \quad (33)$$

The first-order normal breather and Akhmediev breather solutions are derived analytically, and its profile is shown in Fig. 6.

We also give the second-order breather solutions, In this case, we set the parameters in eq. (30) as follows:

$$N = 4, P_1 = -P_2, P_3 = -P_4, Q_1 = Q_2, Q_3 = Q_4, \eta_1^0 = \eta_2^0 = \eta_3^0 = \eta_4^0 = 0, \quad (34)$$

Two different forms of second-order breathers can be seen in Fig. 7. The higher-order breather solutions can also be generated from soliton solutions (30) under parameter constraints (32) and They exhibit richer dynamic behavior. We would not be here continue to investigate this problem.

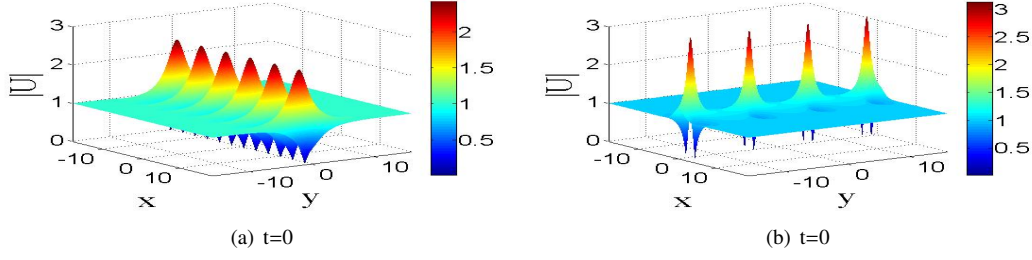


Figure 6: Two kinds of first-order breather solutions on a constant background at time  $t = 0$ , for eq. (3) with the parameters: (a):  $P_1 = \frac{1}{2}, Q_1 = 1$ ; (b):  $P_1 = \frac{i}{2}, Q_1 = \frac{2i}{3}$ .

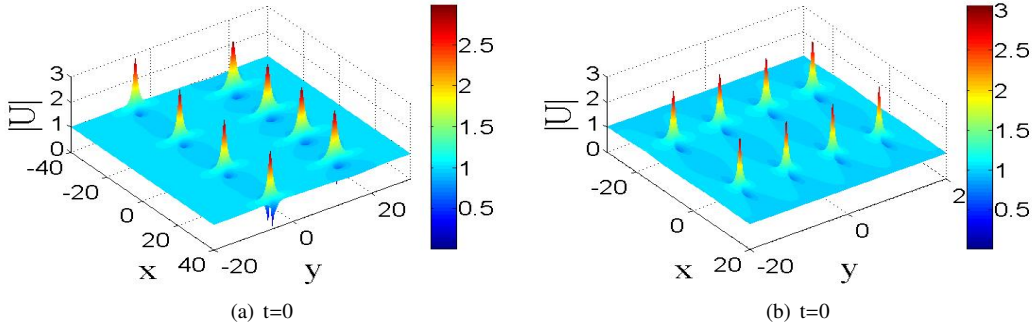


Figure 7: Two kinds of second-order breather solutions on a constant background at time  $t = 0$ , for eq. (3) with the parameters: (a):  $P_1 = \frac{1}{3}, P_3 = \frac{1}{4}, Q_1 = \frac{1}{3}, Q_3 = \frac{1}{3}$ ; (b):  $P_1 = \frac{i}{3}, P_3 = \frac{i}{4}, Q_1 = \frac{2i}{3}, Q_3 = \frac{2i}{3}$ .

### 3.2. Rational and semi-rational solutions

The rational solutions of eq. (3) are generated from breathers given by eq. (30) in the long-wave limit. Taking the parameters in eq. (30) as

$$N = 2, Q_1 = \lambda_1 P_1, Q_2 = \lambda_2 P_2, \lambda_1 = -\lambda_2 = \lambda \neq 0, \quad (35)$$

and taking the limit of  $P_j \rightarrow 0$  ( $j = 1, 2$ ), the first-order rational solution is obtained in the following form

$$U = \frac{2(\lambda y - i\sqrt{2})^2 + 2(x - \lambda\sqrt{2}t)^2 + 1}{2(x - \lambda\sqrt{2}t)^2 + 2\lambda^2 y^2 + 1}, \quad V = \frac{8(x - \lambda\sqrt{2}t)\lambda^2 y}{(x - \lambda\sqrt{2}t)^2 + \lambda^2 y^2 + 1/2}. \quad (36)$$

The corresponding rational solutions are lumps,  $(U, V) \rightarrow (1, 0)$  when  $(x, y)$  goes to infinity at any given time. Lump moves along the line direction defined by  $x - \lambda\sqrt{2}t = 0$ , and reaches the maximum value on this line when  $y = 0$ . The patterns of lump solution do not change, if we modify the time. Without loss of generality, the lump solution  $U$  has the following critical points at time  $t = 0$ :

$$\Lambda_1 = (0, 0); \Lambda_2 = \left(\frac{\sqrt{6}}{2}, 0\right); \Lambda_3 = \left(-\frac{\sqrt{6}}{2}, 0\right); \quad (37)$$

Interestingly, the locality of lump is controlled by the value of  $\lambda$ . As the value of  $|\lambda|$  increases, the localization of the lump will be better (see Fig. 8).

For constructing semi-rational solutions of eq. (3), we first consider semi-rational solutions consisting of first-order Lump and periodic line waves obtained from the 3-soliton solutions. For simplicity, setting

$$N = 3, Q_1 = \lambda_1 P_1, Q_2 = \lambda_2 P_2, \eta_1^0 = \eta_2^{0*} = i\pi, \quad (38)$$

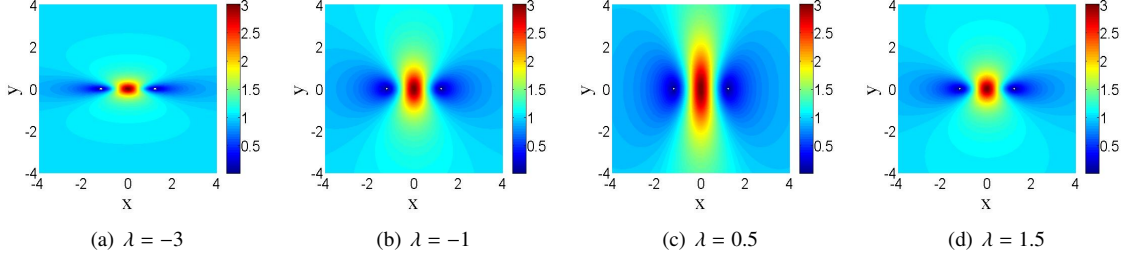


Figure 8: Lump solution  $|U|$  given by Eq. (36) in the  $(x, y)$ -plane at  $t = 0$ .

and  $P_1, P_2 \rightarrow 0$ , then the functions  $\tilde{f}$  and  $\tilde{g}$  can be rewritten as

$$\begin{aligned}\tilde{f} &= -[(x - 3\sqrt{2}t + 2i)^2 + (3y + \sqrt{2})^2 + \frac{1}{2}e^{ix-\pi}] - (3y)^2 - (x - 3\sqrt{2}t)^2 - \frac{1}{2}, \\ \tilde{g} &= -i[(x - 3\sqrt{2}t + 2i)^2 + (3y + \sqrt{2} - \sqrt{2}i)^2 + \frac{1}{2}e^{ix-\pi}] - (3y - \sqrt{2}i)^2 - (x - 3\sqrt{2}t)^2 - \frac{1}{2},\end{aligned}\quad (39)$$

where  $\lambda_1 = -\lambda_2 = 3, P_3 = 1, Q_3 = 0, \eta_3^0 = -\pi$ . This corresponding solution  $|U|$ , which is plotted in Fig. 9, is a hybrid of a lump and periodic line waves. The periodic line waves keep periodic in  $x$  direction and localized in  $y$  direction and the periodic is  $2\pi$ . Compared to the height of the peak of first-order lump on a flat background shown in Fig.8, an interesting phenomenon is that lump does not generate more energy in the background of the periodic background.

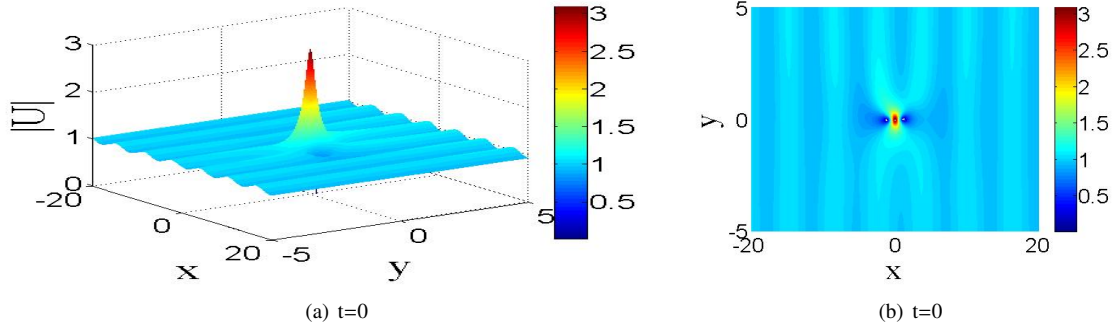


Figure 9: Semi-rational solutions  $|U|$  plotted in the  $(x, y)$ -plane, which consist of lump and periodic line waves with parameters given by eq. (39).

In addition, semi-rational solutions composed of first-order lump and Akhmediev breather can also be obtained, in a similar way, from the 4-soliton solutions. We have to take the parameters

$$N = 4, Q_1 = \lambda_1 P_1, Q_2 = \lambda_2 P_2, \eta_1^0 = \eta_2^{0*} = i\pi, \eta_3^0 = \eta_4^0, \quad (40)$$

and take a limit as  $P_1, P_2 \rightarrow 0$ . Then the functions  $\tilde{f}$  and  $\tilde{g}$  can be rewritten as

$$\begin{aligned}\tilde{f} &= -[A_1 e^{\zeta_1} + B_1 e^{\zeta_2} + C_1 e^{\zeta_3} + D_1], \\ \tilde{g} &= -\left[\sum_{k=1}^3 A_{1k} e^{\zeta_k} + \sum_{k=1}^3 C_{1k} e^{\zeta_k} + (A_{11} + B_{12} + A_{13})e^{\zeta_2} + D_2\right],\end{aligned}\quad (41)$$

Here

$$\begin{aligned}
\zeta_1 &= -\frac{i}{4}x + \frac{1}{3}y - \frac{\sqrt{31}}{12}it - 2\pi, & \zeta_2 &= \frac{i}{4}x + \frac{1}{3}y + \frac{\sqrt{31}}{12}it - 2\pi, & \zeta_3 &= \frac{2}{3}y - 4\pi, \\
A_1 &= [(\sqrt{2}t + x - 8i)^2 + (y - \sqrt{62})^2] + \frac{1}{2}, & B_1 &= [(\sqrt{2}t + x + 8i)^2 + (y - \sqrt{62})^2] + \frac{1}{2}, \\
C_1 &= [\frac{32}{31}(y - 2\sqrt{62})^2 + \frac{32}{31}(x + \sqrt{2}t)^2 + \frac{16}{31}], & C_{12} &= \frac{[(15\sqrt{31}i + 97)(x + \sqrt{2}t)]^2}{124}, \\
A_{11} &= \frac{[(15 + \sqrt{31}i)y - 16(\sqrt{62} + \sqrt{2}i)]^2}{16\sqrt{31}i + 240}, & D_2 &= (y + \sqrt{2}i)^2 + (x - \sqrt{2}t)^2 + \frac{1}{2}, \\
A_{12} &= \frac{[(15\sqrt{2} + \sqrt{62}i)t + (15 + \sqrt{31}i)x + 8\sqrt{31} - 120i]^2}{16\sqrt{31}i + 240}, & C_{13} &= \frac{1455\sqrt{31}i + 1217}{1860\sqrt{31}i + 12028}, \\
B_{12} &= \frac{[(15\sqrt{2} + \sqrt{62}i)t + (15 + \sqrt{31}i)x - 8\sqrt{31} + 120i]^2}{16\sqrt{31}i + 240}, & A_{13} &= \frac{15\sqrt{31}i + 9}{16\sqrt{31}i + 240}, \\
C_{11} &= \frac{[(15\sqrt{31}i + 97)y - (883\sqrt{2}i + 209\sqrt{62}i)]^2}{1860\sqrt{31}i + 12028}, & D_1 &= [(x + \sqrt{2}t)^2 + y^2 + \frac{1}{2}].
\end{aligned} \tag{42}$$

The corresponding semi-rational solution is illustrated in Fig.10; we see that a fundamental lump and an Akhmediev breather coexist on a constant background, and the period of the Akhmediev breather is  $8\pi$ .

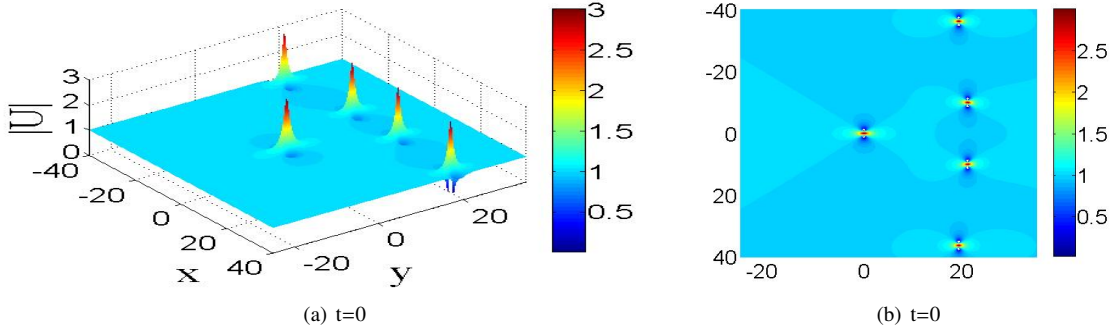


Figure 10: Semi-rational solutions  $|U|$  plotted in the  $(x, y)$ -plane, which consist of lump, and Akhmediev breather for eq. (3) with parameters  $P_3 = -P_4 = \frac{1}{4}, Q_3 = Q_4 = \frac{1}{3}, \eta_3^0 = \eta_4^0 = -2\pi, \eta_5^0 = -2\pi, \lambda_1 = -\lambda_2 = 1$  in Eq. (40).

It is worth noting that whether the reverse space-time 2D nonlocal NLS equation(3) can be reduced to the following reverse space-time 1D nonlocal NLS equation, namely

$$iU(x, t)_t + AU(x, t)_{xx} + BU(x, t)U(x, t)U(-x, -t) = 0$$

is a meaningful issue. We will consider it in a follow-up work.

#### 4. Summary

In this paper,  $N$ -soliton solutions, periodic solutions, rational and semi-rational solutions for the two kinds of 2D nonlocal NLS equations [eqs. (2) and (3)], which features specific  $\mathcal{PT}$  symmetry with respect to different space and time, are derived by means of the Hirota method and long-wave limit. For eq. (2), two types of periodic solutions are obtained analytically. These are line breathers, and the solutions produced by the interplay of line breathers and periodic line waves. The first-order solutions of these two types are displayed in Figs. 1 and 2, respectively. By taking the long-wave limit of these periodic solutions, the W-shaped line RW (rogue-wave) and a semi-rational solution have been constructed analytically, with examples of them plotted in Figs. 3 and 4, respectively. Moreover, the dynamics

of higher-order semi-rational solutions built of RWs and line breathers are presented in detail (see Fig. 5). For eq. (3), the obtained periodic solutions are a normal breather and Akhmediev breather (see Figs. 6 and 7). The nonsingular rational solution is a lump, while the semi-rational states represent first-order lumps built on top of the background of periodic line waves (see Figs. 9). Furthermore, the corresponding semi-rational solutions consisting of the first-order lump and Akhmediev breather are generated (see Figs. 10). The main differences and problems for the solution of eqs.(2) and (3) can be summarized as follows:

- First-order breathers. Eq. (2) produces line breathers, which are line waves periodic in both  $x$  and  $y$  directions. These line breathers disappear after a relatively short evolution time (see Fig. 1). On the other hand, eq. (3) represents usual breathers which are periodic in one direction and localized in the other direction, see Fig. 6.
- Rational solutions. The fundamental rational solution of eq. (2) is a line RW, whose nonvanishing amplitude persists for a very short period of time (see Fig.3). However, the nonsingular rational solution is a lump of eq. (3), which is a local traveling wave keeping a constant amplitude during its propagation, see eq.(36).
- Semi-rational solutions. These solutions to eq. (2) describe the interaction of RWs, line breathers, and periodic line waves, see Figs. 4 and 5. The semi-rational solutions of eq. (3) are composed of lump, breather and periodic line waves, see Figs. 9 and 10.
- The reduction problem. Eq. (2) can be reduced to the “reverse-space” 1D nonlocal NLS equation by a certain transformation. However, we could not produce a  $(1 + 1)$ D reduction of the reverse space-time  $(2 + 1)$ D nonlocal NLS equation (3). Thus, it is interesting to reduce it to a reverse space-time 1D nonlocal NLS equation. This will be considered elsewhere.

These results essentially enrich the diversity of wave structures produced by 2D nonlocal NLS equations. Additionally, the distinctive structure of these 2D solutions is stressed by comparing them to exact solutions of the nonlocal DS I and DS II (Davey-Stewartson) equations [52, 53, 54, 65]. These results demonstrate that the Fokas’  $(2 + 1)$  dimensional nonlocal NLS, in the form of eqs. (2) and (3), is a valuable nonlocal extension of the NLS equation, in addition to the previously known ones, in the form of the nonlocal DS I and DS II equations.

Results reported in this paper provide useful models to understand the new features of nonlinear dynamics of  $\mathcal{PT}$ -symmetric systems [44, 45], including new types of rogue-wave solutions, which may find physical realizations (first of all, in optics [4, 5, 66, 67]). Furthermore, the technique of constructing higher-order rational and semi-rational solutions, developed in this work, can be generalized for other nonlinear evolution equations with  $\mathcal{PT}$ -symmetry.

## 5. Acknowledgments

This work is supported by the NSF of China under Grant No. 11671219, and the K.C. Wong Magna Fund in Ningbo University. The work of B.A.M. is partly supported by grant No. 2015616 from the joint program in physics between the National Science Foundation (US) and Binational Science Foundation (US-Israel). Y. Cao and J. He thank members in their group at the Ningbo University for useful discussions.

## References

### References

- [1] N. Akhmediev, A. Ankiewicz, M. Taki, Phys. Lett. A 373 (2009) 675.
- [2] Y. V. Bludov, V. V. Konotop, N. Akhmediev, Phys. Rev. A 80 (2009) 033610.
- [3] Y. V. Bludov, V. V. Konotop, N. Akhmediev, Eur. Phys. J. Spec. Top. 185 (2010) 169.
- [4] A. Montina, U. Bortolozzo, S. Residori, F. T. Arecchi, Phys. Rev. Lett. 103 (2009) 173901.
- [5] D. R. Solli, C. Ropers, P. Koonath, B. Jalali, Nature(London) 450 (2007) 1054.
- [6] C. Kharif, E. Pelinovsky, A. Slunyaev, Rogue waves in the ocean, Springer, Berlin, 2009.
- [7] W. M. Moslem, Phys. Plasmas 18 (2011) 032301.
- [8] H. Bailung, S. K. Sharma, Y. Nakamura, Phys. Rev. Lett. 107 (2011) 255005.
- [9] D. H. Peregrine, J. Aust. Math. Soc. B 25 (1983) 16.
- [10] Y. Ohta, J. K. Yang, Proc. P. Soc. A 468 (2012) 1716.

- [11] B. L. Guo, L. M. Ling, Q. P. Liu, *Phys. Rev. E* 85 (2012) 026607.
- [12] D. J. Kedziora, A. Ankiewicz, N. Akhmediev, *Phys. Rev. E* 84 (2011) 056611.
- [13] A. Ankiewicz, D. J. Kedziora, N. Akhmediev, *Phys. Lett. A* 375 (2011) 2782.
- [14] P. Dubard, P. Gaillard, C. Klein, V. B. Matveev, *Eur. Phys. J. Spec. Top.* 185 (2010) 247.
- [15] P. Dubard, V. B. Matveev, *Nat. Hazards Earth. Syst. Sci.* 11 (2011) 667.
- [16] N. Akhmediev, A. Ankiewicz, J. M. Soto-Crespo, *Phys. Rev. E* 80 (2009) 026601.
- [17] J. S. He, H. R. Zhang, L. H. Wang, K. Porsezian, A. S. Fokas, *Phys. Rev. E* 87 (2013) 052914.
- [18] J. S. He, S. W. Xu, K. Porsezian, *Phys. Rev. E* 86 (2012) 066603.
- [19] W. Liu, D. Q. Qiu, J. S. He, *Commun. Theor. Phys.* 63 (2015) 525.
- [20] X. Wang, J. L. Cao, Y. Chen, *Phys. Scr.* 90 (2015) 105201.
- [21] X. Wang, Y. Q. Li, F. Huang, Y. Chen, *Commun. Nonlinear Sci. Numer. Simulat.* 20 (2015) 434.
- [22] D. Q. Qiu, J. S. He, Y. S. Zhang, K. Porsezian, *Proc. R. Soc. A* 471 (2015) 20150326.
- [23] L. H. Wang, K. Porsezian, J. S. He, *Phys. Rev. E* 87 (2013) 053202.
- [24] J. G. Rao, L. H. Wang, Y. Zhang, J. S. He, *Commun. Theor. Phys.* 64 (2015) 605.
- [25] M. Onorato, S. Residori, U. Bortolozzo, A. Montinad, F. T. Arecchi, *Phys. Rep.* 528 (2013) 47.
- [26] J. M. Dudley, F. Dias, M. Erkintalo, G. Genty, *Nature Photonics* 8 (2014) 755.
- [27] M. Onorato, S. Residori, F. Baronio, *Rogue and shock waves in nonlinear dispersive media, lecture notes in physics*, Springer, Berlin, 2016.
- [28] Y. Ohta, J. K. Yang, *Phys. Rev. E* 86 (2012) 036604.
- [29] Y. Ohta, J. K. Yang, *J. Phys. A: Math. Theor.* 46 (2013) 105202.
- [30] P. Dubard, V. B. Matveev, *Nonlinearity* 26 (2013) 93.
- [31] G. Mu, Z. Y. Qin, *Nonlinear Anal. Real World Appl.* 18 (2014) 1.
- [32] Y. Zhang, Y. B. Sun, W. Xiang, *Appl. Math. Comput.* 263 (2015) 204.
- [33] J. C. Chen, Y. Chen, B. F. Feng, *Phys. Lett. A* 379 (2015) 1510.
- [34] J. C. Chen, Y. Chen, B. F. Feng, Z. Y. Ma, *Nonlinear Dyn.* 88 (2017) 1273.
- [35] C. Qian, J. G. Rao, Y. B. Liu, J. S. He, *Chin. Phys. Lett.* 33 (2016) 110201.
- [36] J. Cuevas-Maraver, B. A. Malomed, P. G. Kevrekidis, D. J. Frantzeskakis, *Phys. Lett. A* 382 (2018) 968.
- [37] A. S. Fokas, *Nonlinearity* 29 (2016) 319–324.
- [38] M. Dimakos, A. S. Fokas, *J. Math. Phys.* 54 (2013) 081504.
- [39] M. J. Ablowitz, D. J. Kaup, A. C. Newell, H. Segur, *Stud. Appl. Math.* 53 (1974) 249–315.
- [40] C. M. Bender, S. Boettcher, *Phys. Rev. Lett.* 80 (1998) 5243–5246.
- [41] C. M. Bender, D. C. Brody, H. F. Jones, *Phys. Rev. Lett.* 89 (2002) 270401.
- [42] K. G. Makris, R. E. Ganainy, D. N. Christodoulides, Z. H. Musslimani, *Phys. Rev. Lett.* 100 (2008) 103904.
- [43] Z. H. Musslimani, K. G. Makris, R. E. Ganainy, D. N. Christodoulides, *Phys. Rev. Lett.* 100 (2008) 030402.
- [44] V. V. Konotop, J. K. Yang, D. A. Zezyulin, *Rev. Mod. Phys.* 88 (2016) 035002.
- [45] S. V. Suchkov, A. A. Sukhorukov, J. H. Huang, S. V. Dmitriev, C. H. Lee, Y. S. Kivshar, *Laser Photonics Rev.* 10 (2016) 177–213.
- [46] J. K. Yang, *Opt. Lett.* 39 (2014) 113–136.
- [47] Y. V. Kartashov, V. V. Konotop, L. Torner, *Phys. Rev. Lett.* 115 (2015) 193902.
- [48] J. K. Yang, *Phys. Rev. E* 91 (2015) 023201.
- [49] A. Beygi, S. P. Klevansky, C. M. Bender, *Phys. Rev. A* 91 (2015) 062101.
- [50] C. Huang, L. Dong, *Opt. Lett.* 41 (2016) 5194–5197.
- [51] R. Hirota, *The direct method in soliton theory*, Cambridge University Press, 2004.
- [52] J. G. Rao, Y. S. Zhang, A. S. Fokas, J. S. He, *Rogue waves of the nonlocal Davey-Stewartson I equation*. Accepted by *Nonlinearity* (2018)  
DOI: 10.13140/RG.2.2.14395.41766 at Researchgate.
- [53] J. G. Rao, Y. Cheng, J. S. He, *Stud. Appl. Math.* 139 (2017) 568–598.
- [54] J. G. Rao, K. Porsezian, J. S. He, *Chaos* 27 (2017) 083115.
- [55] J. G. Rao, K. Porsezian, J. S. He, T. Kanna, *Proc. R. Soc. A* 474 (2017) 0627.
- [56] E. G. Fan, K. W. Chow, J. H. Li, *Stud. Appl. Math.* 128 (2012) 86–105.
- [57] M. J. Ablowitz, Z. H. Musslimani, *Phys. Rev. Lett.* 110 (2013) 064105.
- [58] M. J. Ablowitz, Z. H. Musslimani, *Nonlinearity* 29 (2016) 915–946.
- [59] X. Huang, L. M. Ling, *Eur. Phys. J. Plus* 131 (2016) 148.
- [60] X. Y. Wen, Z. Yan, Y. Yang, *Chaos* 26 (2016) 063123.
- [61] V. Gerdjikov, A. Saxena, *J. Math. Phys.* 58 (2017) 013502.
- [62] A. K. Sarma, M. A. Miri, Z. H. Musslimani, D. N. Christodoulides, *Phys. Rev. E* 89 (2014) 052918.
- [63] M. Li, T. Xu, *Phys. Rev. E* 91 (2015) 033202.
- [64] T. A. Gadzhimuradov, A. M. Agalarov, *Phys Rev A* 93 (2016) 062124.
- [65] M. J. Ablowitz, Z. H. Musslimani, *Stud. Appl. Math.* 139 (2017) 7–59.
- [66] D. R. Solli, G. Herink, B. Jalali, C. Ropers, *Nat. Photonics* 6 (2012) 463.
- [67] A. Tikan, C. Billet, A. T. G. El, M. Bertola, T. Sylvestre, F. Gustave, S. Randoux, G. Genty, P. Suret, J. M. Dudley, *Phys. Rev. Lett.* 119 (2017) 033901.